AMERICAN JOURNAL OF MATERIALS AND NANOTECHNOLOGY

Effects of CeO_2 on the Si Precipitation Mechanism of SiCp/Al-Si Composite Prepared by Powder Metallurgy

Bin Yang [1,*], Aiqin Wang [1,2], Kunding Liu [1], Chenlu Liu [1], Jingpei Xie [1,2], Guangxin Wang [1] and Shizhong Wei [1]

1 Materials Science and Engineering School, Henan University of Science and Technology, Luoyang 471023, China;

Abstract: SiCp/Al-Si composites with di erent CeO_2 contents were prepared by a powder metallurgy method. The e ect of CeO_2 content on the microstructure of the composites was studied. The mechanism of CeO_2 on the precipitation of Si during sintering was analyzed by theoretical calculations. The results show that the appropriate amount of CeO_2 can significantly refine the size of precipitated Si particles in the composite and increase the number of Si particles. With the increase of CeO_2 content from 0 to 0.6 wt%, the number of Si particles precipitated in the composites increases gradually, and the average particle size of Si particles decreases gradually. When the CeO_2 content is 0.6 wt%, the number of Si particles precipitated in the composites reaches the maximum, and the average particle size reaches the minimum. However, with the increase of CeO_2 content from 0.6 wt% to 1.8 wt%, the number of Si particles precipitated in the composites began to decrease, and the average size of Si particles gradually increased. CeO_2 can be used as heterogeneous nucleation substrate of precipitated Si, and the nucleation rate of precipitated Si on a CeO_2 substrate is higher than that on an aluminum substrate. The proper addition of CeO_2 can improve the nucleation e ciency of precipitated Si, thus increasing the amount and refining the size of precipitated Si.

Keywords: powder metallurgy; rare earth element; precipitated Si; microstructure refinement

1. Introduction

With the development of the modern manufacturing industry, research and development of high-performance materials has become one of the important topics in the development of the aerospace industry [1–3]. In spacecraft design, due to the particularities of the space flight environment, the materials used for the vessel and its auxiliary equipment are usually required to have ultra-high specific strength and toughness, good high-temperature performance and thermal stability, as well as remarkable fatigue resistance, vibration resistance, corrosion resistance, etc. [4–7].

Due to the advantages of low density, high specific strength, low thermal expansion coe cient, good thermal conductivity and high wear resistance, SiC particle reinforced Al-Si matrix composite (SiCp/Al-Si composite) has been widely used in aerospace applications, electronic instruments, military equipment, wear-resistant materials and many other fields [8–12]. SiCp/Al-Si composites prepared by powder metallurgy usually have the following advantages: the distribution of the reinforcement phase is uniform, the content is easy to adjust, the proportion of each component is accurate and there is no obvious agglomeration [13,14]. In addition, due to the low temperature used in the preparation

process, the composites are generally in solid or partial melting state, so the interfacial reaction between matrix and reinforcement is very weak, which reduces the formation of interface impurities and brittle phases [15]. However, for the SiCp/Al-Si composites with high Si content in the matrix, multi-scale precipitation of Si phase will occur during the preparation process, and coarse and irregular Si particles will be precipitated in the matrix [16–18]. These particles can easily split the matrix, reduce the mechanical properties of the materials and restrict the improvement of its physical and mechanical properties. Therefore, it is of great significance to improve the physical and mechanical properties of SiCp/Al-Si composites by reducing or preventing the multi-scale precipitation of a Si phase during the preparation process.

At present, many scholars have studied the application of rare earths as grain refiner in casting Al-Si alloys [19–22]. Compared with other rare earth elements, Ce has been the most investigated due to its relatively low cost and good compatibility with the aluminum matrix. Li et al. [23] found that the addition of 1.0 wt% Ce significantly refined the primary Si and transferred the morphology from coarse irregular to fine blocky. Xue et al. [24] reported that CeO_2 additive could significantly improve the dispersion of in-situ formed TiB_2 in an Al matrix while refining -Al grains. Wu et al. [25] fabricated Ti/Al_2O_3 composites with di erent volume content of CeO_2 via vacuum hot-pressing sintering and found that the addition of CeO_2 could significantly improve the microhardness, flexural strength and fracture toughness. However, there are few reports on the application of CeO_2 in Al-Si alloy and Al-Si alloy matrix composites prepared by powder metallurgy and little attention has been paid to the e ects of CeO_2 on the microstructure of SiCp/Al-Si composites. In this paper, SiCp/Al-Si composites with di erent CeO_2 contents were prepared by a powder metallurgy method, the influence of CeO_2 content on the microstructure of the composites were studied and the mechanism of the influence of CeO_2 on the precipitation of Si phase in the composites was discussed.

2. Experimental Process

The SiCp/Al-Si composites with di erent CeO_2 contents were prepared by a powder metallurgy method. Al-19Si-1.5Cu-0.6Mg alloy powder prepared by the gas-atomization method was used as matrix, SiCp with average particle size of 10 m was selected as reinforcement material and its mass fraction was 20 wt%, The additive used in the experiments was high purity CeO_2 powder, which mass fraction was respectively 0, 0.15 wt%, 0.3 wt%, 0.6 wt%, 1.2 wt%, 1.8 wt%. First, the above powders were mixed by a ball mill (the ratio of balls to powder was 2:1) for 4 h and then dried. Next the mixed powders were cold-rolled to a diameter of 78 mm, length 48 mm billet with 500 MPa pressure in a hydraulic machine; then the billets were heated in a tube furnace, the sintering temperature was 550 °C, sintering time was 3 h (the protective gas was N_2).

The X-ray di raction (XRD) patterns of composites with di erent CeO_2 contents were determined using an X-pertpro X-ray di ractometer (PANalytical, Eindhoven, The Netherlands) with Cu K radiation (k = 0.15406 nm) operated at 40 kV and 100 mA. The microstructure of the samples were observed using scanning electron microscopey (SEM, JSM-5600LV, JEOL, Tokyo, Japan) with energy dispersive spectroscopy (EDS, Kevex, Texas, TX, USA) and transmission electron microscopy (TEM, JEOL JEM-2100). Samples for SEM analysis were prepared via grinding with SiC abrasive papers and polishing with an Al_2O_3 suspension solution and diamond solutions of di erent abrasive sizes (6, 3, 1 and 0.3 m). After metallographic polishing, the samples were corroded by Keller reagent for 30 s. The TEM foil was mechanically polished to about 20 m and further thinned via ion milling with a precision ion polishing system (PIPS, Model 691, Gatan, Pleasanton, CA, USA). The average grain size of Si particles precipitated from the composites with di erent CeO_2 content was measured by Image Pro Plus software v6.0. This software generates histograms of precipitated Si particles from the SEM image and quantifies the diameter of precipitated Si through line profile analysis which provides the average grain size of all precipitated Si particles.

3. Results and Discussion

3. Results and Discussion

3.1. The XRD Analysis of SiCp/Al-Si Composites with Different CeO_2 Contents

3.1. The XRD Analysis of SiCp/Al-Si Composites with Di erent CeO_2 Contents

Figure 1 shows the XRD patterns of SiCp/Al-Si Composites with different CeO_2 contents. It can be seen that all the samples contain the diffraction peaks of Al matrix (JCPDS card No.04–0787), SiC particles (JCPDS card No. 29–1131) and precipitated Si (JCPDS card No. 27–1402). However, due to the relatively low amount of addition and the fact that the diffraction peaks of CeO_2 overlap with those of precipitated Si, the diffraction peak of CeO_2 (JCPDS card No. 34–0394) is only found in the composites with 1.8 wt% CeO_2 content, and the diffraction peak intensity is weak. This shows that CeO_2 added in the composite is relatively stable, and CeO_2 does not react during the preparation process.

Figure 1 shows the XRD patterns of SiCp/Al-Si Composites with di erent CeO contents. It can be seen that all the samples contain the diffraction peaks of Al matrix (JCPDS card No.04–0787), SiC particles (JCPDS card No. 29–1131) and precipitated Si (JCPDS card No. 27–1402). However, due to the relatively low amount of addition and the fact that the diffraction peaks of CeO_2 overlap with those of precipitated Si, the diffraction peak of CeO_2 (JCPDS card No. 34–0394) is only found in the composites with 1.8 wt% CeO_2 content, and the diffraction peak intensity is weak. This shows that CeO_2 added in the composite is relatively stable, and CeO_2 does not react during the preparation process.

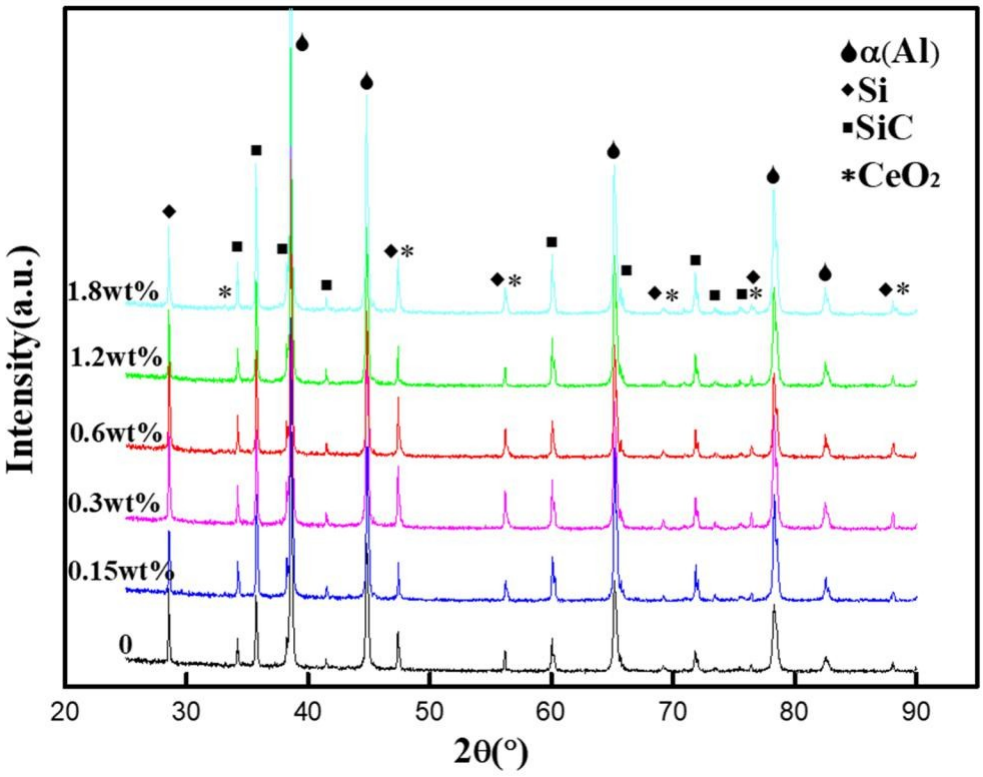

Figure 1. XRD pattern of SiCpSiCp/Al/-Si Composites with didifferentCeO Contents.**Figure1.**XRDpatternof-SiCompositeswithCeO22 Contents.

3.2. E ect of CeO_2 Additions on the Microstructure of SiCp/Al-Si Composites

3.2. Effect of CeO_2 Additions on the Microstructure of SiCp/Al-Si Composites

Figure 2 shows the SEM and EDS images of SiCp/Al-Si Composites with different CeO_2 contents. It can be seen that the microstructure of the composites mainly consists of three phases: a dark gray particle phase (as shown in region A in Figure 2f), a light gray particle phase (as shown in region B in particle phase (as shown in region A in Figure 2f), a light gray particle phase (as shown in region B Figure 2f) and a white particle phase (as shown in region C in Figure 2f). Combining the XRD analysis in Figure 2f) and a white particle phase (as shown in region C in Figure 2f) . Combining the XRD in Figure 1 and the EDS results in Figure 2f–i, it can be concluded that the dark gray particle phase in analysis in Figure 1 and the EDS results in Figure 2f–i, it can be concluded that the dark gray particle

Figure 2 shows the SEM and EDS images of SiCp/Al-Si Composites with different CeO_2 contents.
It can be seen that the microstructure of the composites mainly consists of three phases: a dark gray

the composites is SiCp, the light gray particle phase is precipitated Si and the white particle phase is phase in the composites is SiCp, the light gray particle phase is precipitated Si and the white particle CeO_2.

phase is CeO_2.

The average diameter of Si particles precipitated in the composites with different CeO_2 contents is shown in Figure 3. It can be seen that when the content of CeO_2 is between 0 and 0.6 wt%, the average size of precipitated Si particles gradually decreases with the increase of CeO_2 content, and the number of precipitated Si particles gradually increases; when the content of CeO_2 is between 0.6 wt% and 1.8 wt%, the change trend of average size and number of precipitated Si particles is opposite to the above, the main reason for this phenomenon may be that the agglomeration of CeO_2 increases with the increase of CeO_2 content. When the content of CeO_2 is less than 0.6 wt%, CeO_2 mainly exists in the form of particles, and when the content of CeO_2 is more than 0.6 wt%, the agglomeration of

CeO_2 in the composite increases. Obviously, an appropriate amount of CeO_2 can refine the precipitated Si, When the CeO_2 content is 0.6 wt%, the number of Si particles precipitated in the composites reaches the maximum and the average particle size reaches the minimum.

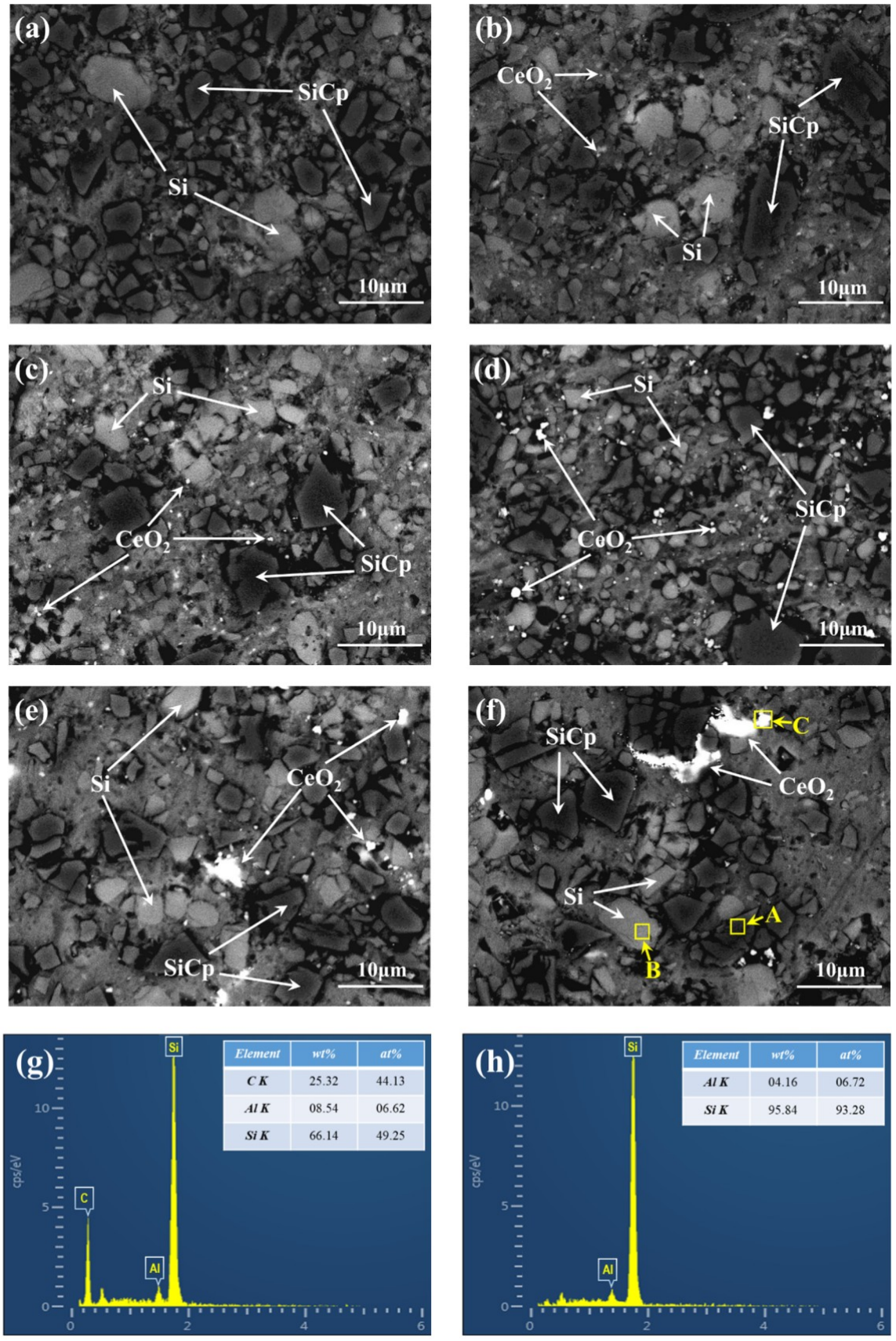

Figure 2. Cont.

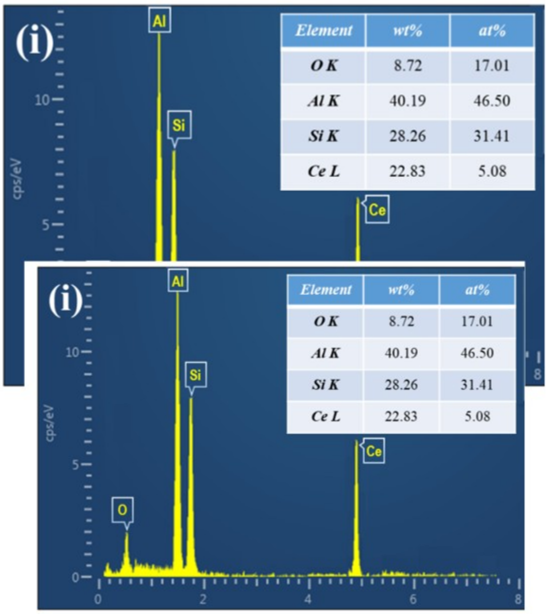

Figure 2. The SEM and EDS pictures of SiCp/Al-Si Composites with di erent CeO_2 Contents: (**a**) 0; (**b**)

Figure 2. The SEM and EDS pictures of SiCp/Al-Si Composites with different CeO_2 Contents: (**a**) 0; 0.15 wt%; (**c**) 0.30 wt%; (**d**) 0.60 wt%; (**e**) 1.20 wt%; (**f**) 1.80 wt%; (**g**) the energy spectrum diagram of (**b**) 0.15 wt%; (**c**) 0.30 wt%; (**d**) 0.60 wt%; (**e**) 1.20 wt%; (**f**) 1.80 wt%; (**g**) the energy spectrum diagram region A in Figure 2f; (**h**) the energy spectrum diagram of region B in Figure 2f; (**i**) the energy spectrum of region A in Figure 2f; (**h**) the energy spectrum diagram of region B in Figure 2f; (**i**) the energy diagram of region C in Figure 2f. spectrum diagram of region C in Figure 2f.

the form of particles, and when the content of CeO is more than 0.6 wt%, the agglomeration of CeO

reducing the growth rate of precipitated Si and refining2 the particles. The calculated results about 2 in thethecompositeaveragediameterincreasesof.SiObviously,precipitatedanin appropriatecompositesareamountconsistentof CeOwith2thecanmicrostructurerefinetheprecipitatedanalysis. Si,

WhenThethemorpholCeO2gicalntentdisfference0.6wt%,of thee precipitatednumberof Si particleswasprecipirelativelyated insmall,the whichcompositesindicatesreaches the maximumthatCeO2 contentandthehasveragelittleeffectparticleonthesizemorphologyreachestheof minprecimumpitated. Si particles.

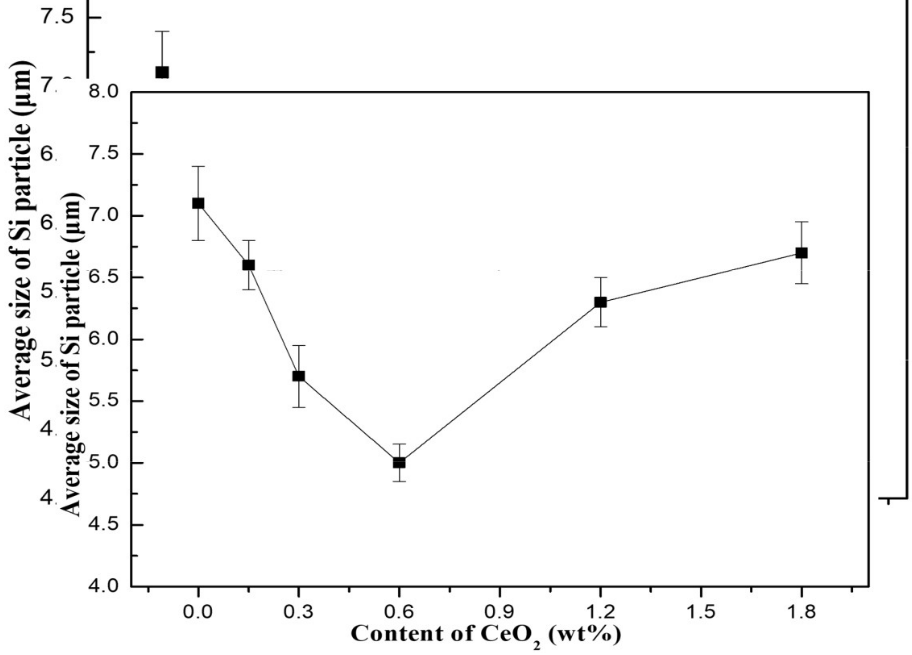

Figure 3. Average size of Si particles precipitated from SiCp/Al-Si composites with different contents of CeO_2.

Figure 3. Average size of Si particles precipitated from SiCp/Al-Si composites with di erent contents of **Figure 3.** Average size of Si particles precipitated from Si*SiCp/Al*-composites with different contents of

3.3. *Influence Mechanism of CeO_2 on the Microstructure of -Si Composites*

CeO .

$^2CeO_2$.

In order to study the influence mechanism of CeO_2 on the size and quantity of precipitated Si in

3.3. *Influence Mechanism of CeO_2 on the Microstructure of SiCp/Al-Si Composites*

the composites, the composite without CeO_2 and the composite with 0.6 wt% CeO_2 content were

In order to study the influence mechanism of CeO_2 on the size and quantity of precipitated Si in the composites, the composite without CeO_2 and the composite with 0.6 wt% CeO_2 content were

The existence of CeO_2 can slow down the di usion of precipitated Si atoms in Al matrix, thus reducing the growth rate of precipitated Si and refining the particles. The calculated results about the average diameter of Si precipitated in composites are consistent with the microstructure analysis. The morphological di erence of the precipitated Si particles was relatively small, which indicates that CeO_2 content has little e ect on the morphology of precipitated Si particles.

3.3. Influence Mechanism of CeO_2 on the Microstructure of SiCp/Al-Si Composites

Materials **2020**, *13*, x FOR PEER REVIEW 6 of 10

analyzed by TEM. Figure 4 shows the TEM microstructure and corresponding electron diffraction in the composites, the composite without CeO and the composite with 0.6 wt% CeO content were patterns of the SiCp/Al-Si composite without CeO_2. After calibration by the software 2MDI jade 5.0, analyzed by TEM. Figure 4 shows the TEM microstructure and corresponding electron diffraction analyzed by TEM. Figure 4 shows the TEM microstructure and corresponding electron di raction the electron diffraction patterns should be Al and precipitated Si, respectively. This indicates that the patterns of the SiCp/Al-Si composite without CeO_2. After calibration by the software MDI jade 5.0, patterns of the SiCp/Al-Si composite without CeO . After calibration by the software MDI jade

Al matrix is the main nucleation substrate for the precipitated 2 Si in the composites without CeO_2 the electron diffraction patterns should be Al and precipitated Si, respectively. This indicates that the 5.0, the electron di raction patterns should be Al and precipitated Si, respectively. This indicates Figure 5 shows the TEM microstructure and corresponding electron diffraction patterns of the Al matrix is the main nucleation substrate for the precipitated Si in the composites without CeO_2. that the Al matrix is the main nucleation substrate for the precipitated Si in the composites without SiCp/Al- Si composite 0.6 wt% CeO_2 content, and diffraction patterns calibration indicated that they Figure 5 shows the TEM microstructure and corresponding electron diffraction patterns of the CeO . Figure 5 shows the TEM microstructure and corresponding electron di raction patterns of should 2 be CeO_2 and precipitated Si, respectively. It can be concluded that in addition to Al matrix as SiCp/Al-Si composite 0.6 wt% CeO_2 content, and diffraction patterns calibration indicated that they the SiCp/Al-Si composite 0.6 wt% CeO content, and di raction patterns calibration indicated that they the nucleation substrate, CeO_2 can also 2 be used as the nucleation substrate for precipitated Si in the should be CeO_2 and precipitated Si, respectively. It can be concluded that in addition to Al matrix as should be CeO and precipitated Si, respectively. It can be concluded that in addition to Al matrix

composites containing CeO.

the nucleation substrate, CeO_2 can also be used as the nucleation substrate for precipitated Si in the as the nucleation substrate, CeO_2 can also be used as the nucleation substrate for precipitated Si in composites containing CeO_2.

the composites containing CeO_2.

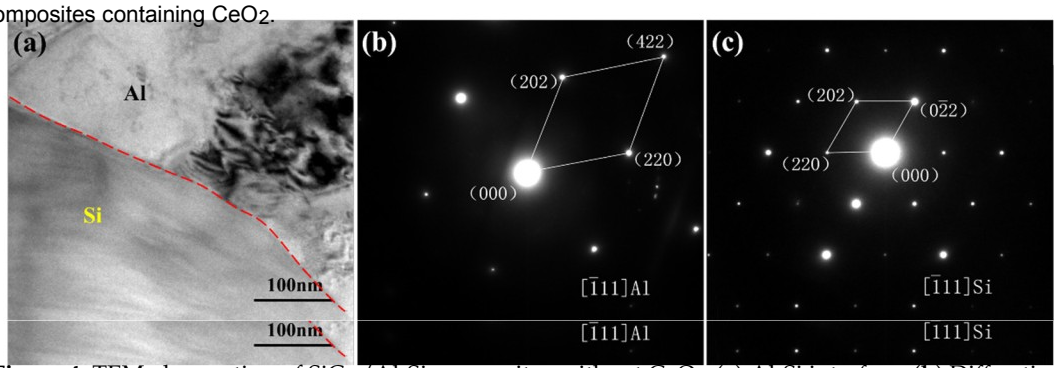

Figure 4. TEM observation of SiCp/Al-Si composites without CeO_2: (**a**) Al-Si interface; (**b**) Diffraction patterns of the Al matrix; (**c**) Di raction patterns of the precipitated Si.

patterns **Figure 4** of. TEM the Al observation matrix; (c) of Diffraction SiCp/Al-Si patterns composites of the without precipitated CeO2: Si (**a**.) Al-Si interface; (**b**) Di raction

Figure 4. TEM observation of SiCp/Al-Si composites without CeO_2: (**a**) Al-Si interface; (**b**) Diffraction patterns of the Al matrix; (**c**) Di raction patterns of the precipitated Si.

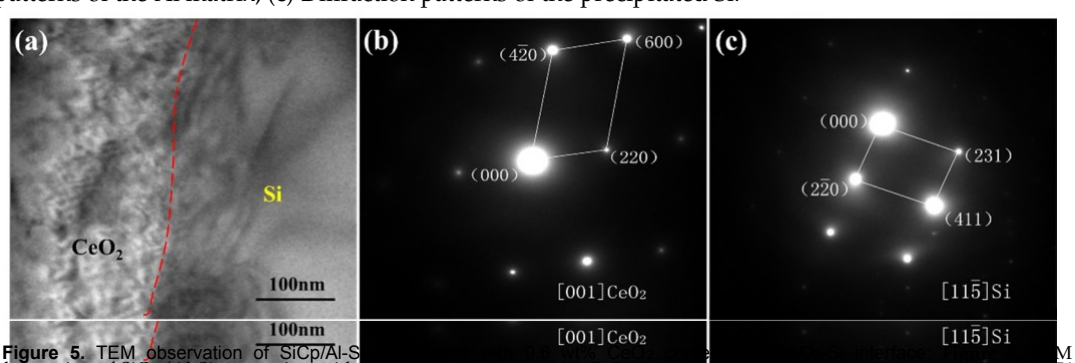

Figure 5. TEM observation of SiCp/Al-Si composites with 0.6 wt% CeO_2 content: (**a**) CeO_2-Si interface; (**b**) Di raction patterns of the CeO_2; (**c**) Di raction patterns of the precipitated Si.

observation of SiCp/Al-Si composites with 0.6 wt% CeO_2 content: (**a**) CeO_2-Si interface; (**b**) Di raction patterns of the CeO_2; (**c**) Di raction patterns of the precipitated Si.

(b) Diffraction patterns of the CeO_2; (c) Diffraction patterns of the precipitated Si.

Figure 5. TEM observation of SiCp/Al-Si composites with 0.6 wt% CeO_2 content: (**a**) CeO_2-Si interface;

(According b) Diffraction to patter the analysis of the of CeO TEM 2; (c) images Diffraction and patterns the corresponding of the precipitated electron Si. di raction patterns of

According to the analysis of TEM images and the corresponding electron diffraction patterns of the the composites, it can be determined that CeO_2 could be used as the nucleation substrate of precipitated composites, it can be determined that CeO2 could be used as the nucleation substrate of precipitated Si, so According to the analysis of TEM im and ges and the corresponding electron diffraction patterns of the

Si, so as to improve the nucleation rate refine the size of precipitated Si particles. Table 1 shows as to improve the nucleation rate and refine the size of precipitated Si particles. Table 1 shows the basic composites, it can be determined that CeO could be used as the nucleation substrate of precipitated Si, so the basic physical parameters of precipitated 2 Si, CeO_2 and Al. It can be seen that the precipitated Si, physical parameters of precipitated Si, CeO_2 and Al. It can be seen that the precipitated Si, CeO_2 and Al as to improve the nucleation rate and refine the size of precipitated Si particles. Table 1 shows the basic CeO_2 and Al matrix belong to the face-centered cubic crystal system. However, the di erence of lattice matrix belong to the face-centered cubic crystal system. However, the difference of lattice constant values physical parameters of precipitated Si, CeO and Al. It can be seen that the precipitated Si, CeO and Al

constant values between precipitated Si and 2 Al is larger than that of precipitated Si and 22 .

between precipitated Si and Al is larger than that of precipitated Si and CeO

matrix belong to the face-centered cubic crystal system. However, the difference of lattice constant values between precipitated Si and Al is larger than that of precipitated Si and CeO_2.

Table 1. Basic physical parameter of Si, CeO_2 and Al.

Phase	Melting Point (K)	Crystal Structure	Lattice Constant (Å)
Si	1673	FCC	0.6636
CeO_2	2873	FCC	0.5411
Al	933	FCC	0.4050

Turnbull and Vonnegut first proposed that the heterogeneous nucleation e ciency of nucleation substrate depends on the lattice mismatch between the nucleation substrate and the nucleation phase [26]. The theory holds that the smaller the mismatch degree between nucleation substrate and nucleation phase is, the more lattice matching between nucleation substrate and nucleation phase is, and the energy caused by lattice mismatch between nucleation substrate and nucleation phase is smaller, too. That is, the smaller the interface energy between nucleation substrate and nucleation phase is, the higher nucleation rate of nucleation phase is. Because the precipitated Si, CeO_2 and Al are face centered cubic structure, the mismatch degree of precipitated Si and two nucleation substrates can be expressed by one-dimensional mismatch degree:

$$= ja_s \quad a_nj/a_n \tag{1}$$

In Equation (1), a_s is the lattice constant of nucleation substrate, Å; and a_n is the lattice constant of nucleation phase, Å. Substituting the values in Table 1 into Equation (1), the calculation shows that the mismatch degree of precipitated Si and CeO_2 is 0.22, and that of precipitated Si and Al is 0.64. According to the lattice mismatch theory, it can be concluded that the nucleation rate of the precipitated Si with CeO_2 as the nucleation substrate is greater than that with Al as the nucleation substrate because the mismatch degree of the precipitated Si and CeO_2 is less than that of the precipitated Si and Al. In addition, according to the crystal growth theory of solid phase transformation [27], the growth mechanism of precipitated Si is mainly di usion-controlled growth. Although the content of CeO_2 in the composites is relatively low, the existence of CeO_2 can still slow down the di usion of precipitated Si atoms in Al matrix, thus reducing the growth rate of precipitated Si and refining the particles.

3.4. Calculation of Nucleation Rate of Precipitated Si in Composites

The Al-Si alloy powder used in this study is supersaturated solid solution prepared by rapid solidification method, the precipitation process of solid solution Si during sintering is a solid phase transformation process, and the nucleation process of precipitated Si in composite materials belongs to heterogeneous nucleation. Compared with homogeneous nucleation, heterogeneous nucleation requires less energy, the formula of free energy di erence in heterogeneous nucleation system is as follows:

$$DG_i = VDG_V + A_{\ i} + VDG_{si} \quad DG_{di} \tag{2}$$

In Equation (2), DG_i is the system free energy, J; DG_V is the unit volume free energy of precipitated Si, J/cm^3; V is the volume of precipitated Si particles, cm^3; $_i$ is the unit area interface energy between the precipitated Si and the nucleation substrate, J/cm^2; A is the interface area, cm^2; DG_{si} is the unit volume elastic strain energy, J/cm^3; and DG_{di} is the surface energy at defects, J.

It is generally believed that VDG_V is nucleation driving force, $A_{\ i} + VDG_{si}$ is resistance to nucleation, and DG_{di} is the surface energy at non-equilibrium defects, which contributes to nucleation work and promotes nucleation. For the convenience of calculation, it is assumed that the interface area between nucleation and nucleation substrate is equal to the surface area of nucleation, therefore, DG_{di} can be expressed as:

$$DG_{di} = A_{\ i} \tag{3}$$

where $_i$ is the unit area surface energy of di erent nucleation substrates, J/cm^2. Hence, Equation (2) can be rewritten as:

$$DG_i = VDG_V + A_i + VDG_{si} \quad A_i \tag{4}$$

Therefore, the critical nucleation size r_{ki} and the critical nucleation Energy DG_{ki} of precipitated Si could be identified as Equations (5) and (6):

$$r_{ki} = 2(_i \quad _i)/(DG_V \quad DG_{si}) \tag{5}$$

$$DG_{ki} = 16 (_i \quad _i)^3/3(DG_V \quad DG_{si})^2 \tag{6}$$

The nucleation rate for heterogeneous nucleation could be identified as Equation (7):

$$N_i = N_0 \exp\frac{DG_{ki}}{kT}\exp\frac{DG_A}{kT} \tag{7}$$

In Equation (7), N_i is the nucleation rate of di erent nucleation substrates, 1/(s cm^3); k is Boltzmann's constant, T is absolute temperature, K; DG_A is the di usion activation energy, J; and N_0 is the atomic number of precipitated Si per unit volume, 1/(s cm^3). Substituting Equation (6) into Equation (7), then the Equation (8) can be rewritten as:

$$N_i = \frac{N_0 kT}{h}\exp\frac{\frac{16 (_i \quad _i)^3}{3(DG_V \quad DG_{si})^2}}{kT}\exp\frac{DG_A}{kT} \tag{8}$$

where h is Planck constant.

Table 2 shows the parameter values for the nucleation of precipitated Si. According to the data in Table 2, it can be calculated that $N_{CeO2} = 4.66\ 10^{12}$(s cm^3) ^{1}, $N_{Al} = 3.33\ 10^{12}$(s cm^3) ^{1}, $N_{CeO2} > N_{Al}$. Therefore, it can be concluded by calculation that the nucleation rate of precipitated Si on CeO_2 substrate is higher than that on Al substrate. However, it should be noted that the nucleation rate of precipitated Si on CeO_2 substrate is not much higher than that on Al substrate. Because of the value of areal surface energy $_i$ for Al matrix (1 10 ^{4}) is higher than that of CeO_2 (1 10 ^{5}), it can be concluded by Equation (5) that the critical radius of Si with CeO_2 as nucleation substrate is smaller than that with Al matrix as nucleation substrate. The decrease of the critical nucleation radius of precipitated Si will lead to the decrease of critical nucleation energy and the increase of nucleation rate. This is consistent with our calculation. The addition of CeO_2 can not only provide more nucleation substrates for precipitated Si to improve the nucleation rate, so as to refine the size and increase the number of precipitated Si particles. Combined with the previous analysis, it can be concluded that when the content of CeO_2 is less than 0.6 wt%, the refining e ect is gradually enhanced with the increase of CeO_2 content, which happens because there are more and more CeO_2 as the nucleation substrate of precipitated Si, and the existence of CeO_2 can slow down the di usion of precipitated Si atoms in Al matrix, thus reducing the growth rate of precipitated Si and refining the particles. However, When the content of CeO_2 is higher than 0.6 wt%, the refining e ect is gradually weakened, which is due to the relatively serious agglomeration phenomenon caused by excessive CeO_2 content, weakens the ability of hindering the growth of precipitated Si, and reduces the refining e ect.

Table 2. The parameter value for the nucleation of precipitated Si on di erent nucleation substrates.

Parameter Value		Nucleation Substrates	
		Al Matrix	CeO_2
DGv	(J/cm^3)	10^4	10^4
DG_A	(J)	2.19 10 19	2.19 10 19
DG_{si}	(J/cm^3)	0	15
N_0	(($s\ cm^3$) 1)	3.94 10^{21}	3.94 10^{21}
i	(J/cm^2)	4 10^6	6 10^6
i	(J/cm^2)	1 10^4	5 10^5
k	(J/k)	23	23
		1.38 10	1.38 10
h	(J s)	6.62 10 34	6.62 10 34
T	(K)	823	823

4. Conclusions

(1) SiCp/Al-Si composites with di erent CeO_2 contents were successfully prepared by a powder metallurgy method. When the content of CeO_2 is less than 0.6 wt%, CeO_2 mainly exists in the form of discrete particles and when the content of CeO_2 is more than 0.6 wt%, the agglomeration of CeO_2 increases.

(2) An appropriate amount of CeO_2 can obviously refine the size of precipitated Si particles and increase the amount of Si particles. With the increase of CeO_2 content from 0 to 1.8 wt%, the number of precipitated Si particles first increases and then decreases, and the average size of precipitated Si particles first increases and then decreases, too. When the CeO_2 content is 0.6 wt%, the number of Si particles precipitated in the composites is the largest and the average size is the smallest.

(3) For the composite without CeO_2, the nucleation of precipitated Si is mainly based on Al matrix. The addition of CeO_2 can be used as the heterogeneous nucleation substrate for precipitated Si, which improves the nucleation rate of precipitated Si. Moreover, the nucleation rate of precipitated Si on CeO_2 substrate is higher than that on Al substrate, which further improves the nucleation rate of precipitated Si, thus increasing the number of precipitated Si particles and refining the size of precipitated Si particles.

Author Contributions: Methodology, software, investigation, and data curation, B.Y. and A.W.; supervision, J.X., and S.W.; formal analysis, K.L. and C.L.; validation and resources, B.Y. and G.W. All the authors discussed the data and wrote the manuscript. All authors have read and agreed to the published version of the manuscript.

Funding: This research was funded by National Natural Science Foundation of China (51801055, 51771070), National Science and Technology Major Project of China (2017ZX02408003), Henan Provincial Department of Science and Technology Research Project (182102210288), Key Scientific Research Projects of Higher Education Institutions of Henan Province (16A430017), Postdoctoral Research Grant in Henan Province (001703039).

Conflicts of Interest: The authors declare no conflict of interest.

References

1. Ezugwu, R.A.; Bonney, V.; Yamane, Y. An overview of the machinability of aeroengine alloys. Mater. Chem. Phys. **2008**, 108, 283–289. [CrossRef]
2. Guo, X.; Wang, L.; Wang, M.; Qin, J.; Zhang, D.; Lu, W. E ects of degree of deformation on the microstructure, mechanical properties & texture of hybrid-reinforced titanium matrix composites. Acta Mater. **2012**, 60, 2656–2667. [CrossRef]
3. Luedtke, A. Thermal management materials for high-performance applications. Adv. Eng. Mater. **2004**, 6, 142–144. [CrossRef]
4. Crouch, I.G. Body armour—New materials, new systems. Def. Technol. **2019**, 15, 241–253. [CrossRef]

5. Tjong, S.C. Recent progress in the development and properties of novel metal matrix nanocomposites reinforced with carbon nanotubes and graphene nanosheets. Mater. Sci. Eng. R Rep. **2013**, 74, 281–350. [CrossRef]
6. Hooker, J.A.; Doorbar, P.J. Metal matrix composites for aeroengines. Mater. Sci. Technol. **2000**, 16, 725–731. [CrossRef]
7. Vasantha, K.P.; Sekar, K.; Venkatesh, K. Recent developments in powder metallurgy based aluminium alloy composite for aerospace applications. Mater. Today **2019**, 18, 5400–5409. [CrossRef]
8. Ghasali, E.; Yazdani-Rad, R.; Asadian, K.; Ebadzadeh, T. Production of Al-SiC hybrid composites using pure and 1056 aluminum powders prepared through microwave and conventional heating methods. J. Alloys Compd. **2017**, 690, 512–518. [CrossRef]
9. Veillère, A.; Kurita, H.; Kawasaki, A.; Lu, Y.; Heintz, J.-M.; Silvain, J.-F. Aluminum/Carbon Composites Materials Fabricated by the Powder Metallurgy Process. Materials **2019**, 12, 4030. [CrossRef]
10. Yang, Y.; Lan, J.; Li, X. Study on bulk aluminium matrix nano-composite fabricated by ultrasonic dispersion of nano-sized SiC particles in molten aluminium alloy. Mater. Sci. Eng. A **2004**, 380, 378–383. [CrossRef]
11. Singh, S.; Pal, K. E ect of texture evolution on mechanical and damping properties of SiC/ZnAl2O4 composite through friction stir processing. J. Mater. Res. Technol. **2018**, 338–350. [CrossRef]
12. Urena, A.; Martinez, E.E.; Rodrigo, P.; Gil, L. Oxidation treatments for SiC particles used as reinforcement in aluminium matrix composites. Comp. Sci. Technol. **2004**, 64, 1843–1854. [CrossRef]
13. Shin, S.; Cho, S.; Lee, D.; Kim, Y.; Lee, S.-B.; Lee, S.-K.; Jo, I. Microstructural Evolution and Strengthening Mechanism of SiC/Al Composites Fabricated by a Liquid-Pressing Process and Heat Treatment. Materials **2019**, 12, 3374. [CrossRef] [PubMed]
14. Zare, R.; Sharifi, H.; Reza Saeri, M.; Tayebi, M. Investigating the e ect of SiC particles on the physical and thermal properties of Al6061/SiCp composite. J. Alloys Compd. **2019**, 801, 520–528. [CrossRef]
15. Mckimpson, M.G.; Scott, T.E. Processing and properties of metal matrix composites containing discontinuous reinforcement. Mater. Sci. Eng. A **1989**, 107, 93–106. [CrossRef]
16. Bai, M.; Xue, Q. Investigation of wear mechanism of SiC particulate-reinforced Al-20Si-3Cu-1Mg aluminium matrix composites under dry sliding and water lubrication. Tribol. Int. **1997**, 30, 261–269. [CrossRef]
17. Molina, J.M.; Narciso, J.; Weber, L.; Mortensen, A.; Louis, E. Thermal conductivity of Al-SiC composites with monomodal and bimodal particle size distribution. Mater. Sci. Eng. A **2008**, 480, 483–488. [CrossRef]
18. Selvam, D.R.; Robinson, J.; Dinaharan, D.S. Syntheses and characterization of Al6061-fly ash-SiC composites by stir casting and compocasting methods. Energy Procedia **2013**, 34, 637–646. [CrossRef]
19. Shi, C.; Zhang, L.; Wu, G.; Zhang, X.; Cheng, A.; Tao, J. E ects of Sc addition on the microstructure and mechanical properties of cast Al-3Li-1.5Cu-0.15Zr alloy. Mater. Sci. Eng. A **2017**, 680, 232–238. [CrossRef]
20. Mao, F.; Yan, G.; Xuan, Z.; Cao, Z.; Wang, T. E ect of Eu addition on the microstructures and mechanical properties of A356 aluminium alloys. J. Alloys Compd. **2015**, 650, 896–906. [CrossRef]
21. Tsai, Y.; Lee, S.; Lin, C.K. E ect of trace Ce addition on the microstructures and mechanical properties of A356 (Al–7Si–0.35 Mg) aluminum alloys. J. Chin. Inst. Eng. **2011**, 34, 609–616. [CrossRef]
22. Li, H.; Gao, Z.; Yin, H.; Jiang, H.; Su, X.; Bin, J. E ects of Er and Zr additions on precipitation and recrystallization of pure aluminium. Scr. Mater. **2013**, 68, 59–62. [CrossRef]
23. Li, Q.; Xia, T.; Lan, Y.; Zhao, W.; Fan, L.; Li, P. E ect of rare earth cerium addition on the microstructure and tensile properties of hypereutectic Al-20% Si alloy. J. Alloys Compd. **2013**, 562, 25–32. [CrossRef]
24. Xue, J.; Wang, J.; Han, Y.F.; Li, P.; Sun, B.D. E ects of CeO_2 additive on the microstructure and mechanical properties of in situ TiB_2/Al composite. J. Alloys Compd. **2011**, 509, 1573–1578. [CrossRef]
25. Wu, C.; Wang, Z.; Li, Q.G.; Shi, G.P.; Liu, M.J.; Li, Y.Y. Mechanical properties and microstructure evolution of Ti/Al_2O_3 cermet composite with CeO_2 addition. J. Alloys Compd. **2014**, 617, 729–733. [CrossRef]
26. Turnbull, D.; Vonnegut, B. Nucleation Catalysis. Ind. Eng. Chem. **1952**, 44, 1292–1298. [CrossRef]
27. Liu, F.; Song, S.J.; Xu, J.F.; Wang, J. Determination of nucleation and growth modes from evaluation of transformed fraction in solid-state transformation. Acta Mater. **2008**, 56, 6003–6012. [CrossRef]